Nanoscale Advances

ROYAL SOCIETY OF CHEMISTRY

PAPER

View Article Online
View Journal | View Issue

Cite this: *Nanoscale Adv.*, 2023, **5**, 6449

Boosted ability of ZIF-8 for early-stage adsorption and degradation of chemical warfare agent simulants†

Sojin Oh, Sujeong Lee, Gihyun Lee and Moonhyun Oh *

Efficient adsorption of hazardous substances from the environment is crucial owing to the considerable risks they pose to both humans and ecosystems. Consequently, the development of porous materials with strong adsorption capabilities for hazardous substances, such as chemical warfare agents (CWAs), is pivotal for safeguarding human lives. Specifically, the early-stage adsorption proficiency of the adsorbents plays a vital role in determining their effectiveness as ideal adsorbents. Herein, we report the efficient adsorption of CWA simulants using thermally treated ZIF-8 (T-ZIF-8). The T-ZIF-8 samples were prepared by subjecting ZIF-8 to a simple thermal treatment, which resulted in a more positive surface charge with extra open metal sites. Although the pore volume of T-ZIF-8 decreased after thermal treatment, the positive surface charge of T-ZIF-8 proved advantageous for the adsorption of the CWA simulants. As a result, the adsorption capacity of T-ZIF-8 for the CWA simulants improved compared to that of pure ZIF-8. Notably, T-ZIF-8 exhibited a remarkably enhanced adsorption ability in the early stage of exposure to the CWA simulants, possibly due to the effective polar interactions between T-ZIF-8 and the simulants *via* the electron-rich components within the CWA simulants. Moreover, the enhanced adsorption capacity of T-ZIF-8 led to the fast degradation of simulant compared to pure ZIF-8. T-ZIF-8 also demonstrated excellent stability over three adsorption cycles. These findings highlight that T-ZIF-8 is an outstanding material for the early-stage adsorption and degradation of CWA simulants, offering high effectiveness and stability.

Received 22nd September 2023
Accepted 5th October 2023

DOI: 10.1039/d3na00807j

rsc.li/nanoscale-advances

1. Introduction

Metal–organic frameworks (MOFs) are an interesting class of porous materials that have garnered considerable attention owing to their unique properties and applications in various fields.[1–28] These materials comprise metal ions or clusters linked by organic ligands, resulting in highly porous structures with large surface areas and tunable pore sizes. MOFs have a wide range of applications in gas storage, catalysis, sensing, adsorption, and separation.[1–28] In particular, the use of MOFs for the adsorption and separation of toxic chemicals including chemical warfare agents (CWAs) is of utmost importance.[15–28]

CWAs can trigger an immense long-term damage to humans and the environment.[15–39] Isopropyl methylphosphonofluoridate known as sarin and bis(2-chloroethyl)sulfide known as sulfur mustard are well-known examples of highly toxic CWAs.[21–28] For examples, sarin inhibits acetylcholinesterase and provokes muscle contraction and asphyxiation,[21–26] and sulfur mustard damages exposed skin and tissue.[24–28] Despite efforts to protect humans from the dangers of CWAs, their use in military activities or terrorist attacks remains prevalent. Therefore, developing efficient and effective methods for the removal and detoxification of CWAs from contaminated air and water is urgently required to protect humans from the adverse effects of CWAs.[15–42] Adsorption is one such effective method, and porous materials, such as porous carbons, zeolites, and MOFs, have shown promising potential in this field.[15–35] In particular, MOFs exhibit outstanding adsorption properties, making them promising candidates for CWA removal.[15–28] Several studies have recently been conducted to explore the potential of MOFs for the adsorption and removal of CWAs.[15–39] Developing porous adsorptive materials for effective adsorption of CWAs is crucial, and the use of MOFs in this context holds tremendous promise. In particular, an effective adsorption ability during the early stage of exposure to CWAs is critical in deeming an adsorbent ideal for use. The simulant compounds that have functionalities similar to those of CWAs but are less toxic and easier to handle are convenient for use in a laboratory. In general, 2-chloroethyl ethyl sulfide (CEES) and dimethyl methyl phosphonate (DMMP) were used as CWA simulants for the study.

Herein, we report the recent developments in the effective adsorption of CWA simulants using ZIF-8. The T-ZIF-8 samples (where *T* denotes the temperature), which have relatively high positive surface charges with extra open metal sites, were

Department of Chemistry, Yonsei University, 50 Yonsei-ro, Seodaemun-gu, Seoul 03722, Republic of Korea. E-mail: moh@yonsei.ac.kr; Fax: +82-2-364-7050; Tel: +82-2-2123-5637

† Electronic supplementary information (ESI) available. See DOI: https://doi.org/10.1039/d3na00807j

prepared by simple thermal treatment of ZIF-8. T-ZIF-8 displayed enhanced adsorption capacity for CWA simulants. Although the pore volume of T-ZIF-8 decreased after thermal treatment, the positive surface charge of T-ZIF-8 were beneficial for the adsorption of the CWA simulants. In particular, a dramatically enhanced adsorption ability of T-ZIF-8 was observed in the early stage of exposure to CWA simulants, possibly because of the effective polar interaction of T-ZIF-8 with the simulants *via* electron-rich moieties within the simulants. Moreover, T-ZIF-8 showed excellent stability during the three adsorption cycles. Not only the boosted ability for the rapid adsorption of simulant but also the enhanced ability for the degradation of simulant were demonstrated by T-ZIF-8. These findings suggest that T-ZIF-8 is an excellent material for the rapid adsorption and degradation of CWA simulants in the early stage of exposure, with high effectiveness and stability.

2. Experimental section

2.1. Materials and characterizations

All solvents and chemicals were purchased from commercial sources and used as received, unless stated otherwise. Deionized water was obtained from a Millipore Direct-Q®3. Scanning electron microscopy (SEM) images were acquired using a JEOL JSM-7001F field-emission scanning electron microscope (Yonsei Center for Research Facilities, Yonsei University). Energy-dispersive X-ray (EDX) spectra were obtained using a Hitachi SU 1510 SEM device equipped with a Horiba EMAX Energy E-250 EDX system. Powder X-ray diffraction (PXRD) patterns were obtained using a Rigaku Ultima IV instrument equipped with a graphite monochromated Cu Kα radiation source (40 kV, 40 mA). The adsorption–desorption isotherms of N_2 (77 K) were measured using a BELSORP Max volumetric adsorption equipment system. All isotherms were measured after pretreatment under a dynamic vacuum at 25 °C for 3 h. X-ray photoelectron spectroscopy (XPS) was conducted using a Thermo Scientific K-Alpha KA1066 spectrometer with a monochromatic Al Ka X-ray source ($h\nu = 1486.6$ eV). The XPS spectra were calibrated with the measured C 1s peak position at 284.6 eV. Zeta-potential measurements were performed in an aqueous solution using a Malvern Nano-ZS Zetasizer. Water contact angle measurements of the prepared pellet samples were performed using a contact angle meter (Biolin Scientific ThetaLite 100) at 25 °C. Water was slowly dropped onto the pellet using a microsyringe, and the contact angle was measured. ^{1}H NMR and ^{31}P NMR spectra were recorded on a Bruker Avance III HD 300 spectrometer (^{1}H NMR, 300 MHz) (^{31}P NMR, 122 MHz), with chemical shifts reported relative to the residual deuterated solvent peaks. The infrared (IR) spectra of the solid samples and liquid CWA simulants were acquired using a Jasco FT/IR 4200 spectrometer and an attenuated total reflection module.

2.2. Preparation of ZIF-8

$Zn(NO_3)_2 \cdot 6H_2O$ (0.1 mmol, 29.7 mg), 2-methylimidazole (5.5 mmol, 451.6 mg), and hexadecyltrimethylammonium bromide (0.0014 mmol, 0.5 mg) were dissolved in 8 mL of deionized water. The resulting aqueous solutions were incubated at room temperature for 20 min. The resulting product was isolated and subsequently washed several times with deionized water and methanol *via* a centrifugation–redispersion cycle and dried under vacuum for 1 h.

2.3. Preparation of T-ZIF-8 samples

Pure ZIF-8 was placed in a tube furnace, heated at 450, 500, 550, 570, or 600 °C for 5 h at a heating rate of 5 °C min^{-1} under N_2 gas flow, and then cooled to room temperature. The resulting products are denoted as T-ZIF-8s, where T denotes the thermal treatment temperature.

2.4. Adsorption of CWA simulants on ZIF samples

The adsorption of 2-chloroethyl ethyl sulfide (CEES) and dimethyl methylphosphonate (DMMP) was performed at room temperature using a jar-in-jar setup. To conduct the experiments, pure ZIF-8 and T-ZIF-8 powders (5.0 mg) were placed in a ceramic crucible pan, and a CWA simulant (2 mL) was taken in a 5 mL beaker. Subsequently, the ceramic crucible pan and beaker were placed in a large jar with the lid closed. The quantity of the CWAs simulants adsorbed onto ZIF-8 or T-ZIF-8s at different time intervals was measured using ^{1}H NMR spectroscopy with CH_2Br_2 as an internal standard. The samples were digested in a mixed deuterated solvent of dimethyl sulfoxide-d_6 and acetic acid-d_4 to obtain ^{1}H NMR spectra.

2.5. Recycling of 550-ZIF-8 for CEES adsorption

Three cycles were conducted in the recycling experiment of 550-ZIF-8 for the adsorption of CEES. After 4 h, in the first adsorption step, 550-ZIF-8 was washed several times with methanol and dried under vacuum for 1 h. The adsorption procedure for the second and third cycles was performed under conditions identical to those of the first adsorption cycle.

2.6. Adsorption kinetics of ZIF samples

The kinetics of the adsorption process provides essential information about reaction path and the rate of adsorbate.[43–46] The pseudo-first order model is one of the representative models. The pseudo-first order model equation is as follows:

$$q_t = q_e(1 - e^{-kt})$$

where, q_e is equilibrium adsorption capacity (mg g^{-1}), q_t is the adsorption capacity (mg g^{-1}) at time t and k is the pseudo-first order rate constant (h^{-1}). The adsorption of CWA simulants was fitted well with pseudo-first order model.

2.7. Degradation of DMMP on ZIF samples

For the degradation of DMMP on ZIF samples, DMMP solution was prepared by mixing DMMP (6 μL) and 3 mL of H_2O and D_2O mixture ($H_2O : D_2O = 9 : 1$ v/v). And then, DMMP solution was added to a 20 mL glass vial containing 100 mg of pure ZIF-8 or 550-ZIF-8. This mixture was continuously stirred at 60 °C. Every several hours, 300 μL of aliquot of the solvent was transferred

into the NMR tube for ^{31}P NMR measurements to determine the conversion of DMMP to MPA. The conversion was then calculated as the ratio of the integrated peak for MPA (the only hydrolysis product) to that of DMMP. After 72 h, the yields for the production of MPA were 67 and 26%, respectively, in the presence of 550-ZIF-8 and pure ZIF-8. Furthermore, the conversion of DMMP to MPA was confirmed by ^{1}H NMR and ^{31}P NMR (see ESI†). For comparison, the degradation of dimethyl 4-nitrophenylphosphate (DMNP) on 550-ZIF-8 was also conducted. For the degradation of DMNP on a ZIF sample, 2.1 mL of 0.45 M *N*-ethylmorpholine buffer solution was added to a 20 mL glass vial containing 50 mg of 550-ZIF-8 and then sonicated for 1 min to disperse homogeneously. After that, 4 μL of DMNP was added and the reaction was continuously stirred at room temperature. Every several hours, 200 μL of aliquot of the solvent was transferred into the NMR tube for ^{31}P NMR measurements to determine the conversion of DMNP.

3. Results and discussion

3.1. Preparation of ZIF-8 and T-ZIF-8 samples

First, cubic ZIF-8 with exposed {100} planes was homogeneously synthesized *via* the reaction of $Zn(NO_3)_2$ and 2-methylimidazole in the presence of hexadecyltrimethylammonium bromide.[47,48] The as-synthesized ZIF-8 was examined using scanning electron microscopy (SEM) to validate the production of consistent ZIF-8 cubes (Fig. 1a). The formation of crystalline ZIF-8 was verified using powder X-ray diffraction (PXRD). The PXRD pattern of the as-synthesized product displayed a representative pattern for ZIF-8 (Fig. 1g). In addition, the expected elements of ZIF-8, including zinc, carbon, and nitrogen, were detected in the energy-dispersive X-ray (EDX) spectrum (Fig. S1†). After confirming the formation of the ZIF-8 cubes, they were thermally treated in a conventional tube furnace at various temperatures (450, 500, 550, 570, and 600 °C) under N_2 gas flow (Fig. 2). Hereafter, samples obtained after thermal treatment of ZIF-8 are designated with the treatment temperature, *i.e.*, 550-ZIF-8 represents ZIF-8 obtained after thermal treatment at 550 °C. Typically, subjecting an MOF to thermal treatment at low temperatures causes the decomposition of some organic linkers, while maintaining the original structure. This process also leads to the creation of positively charged open metal sites.[49–55] However, when the MOF is subjected to high temperature and exposed to an inert gas during thermal treatment, it undergoes complete decomposition and carbonization.[56–61] The SEM images of all T-ZIF-8 samples displayed no morphological changes, despite the thermal treatment involved (Fig. 1). In addition, no critical structural changes were observed, as confirmed by the PXRD patterns of the T-ZIF-8 samples, except for 570-ZIF-8 and 600-ZIF-8 (Fig. 1g). Photographs of 450, 500, and 550-ZIF-8 displayed only minor color changes from white to beige (insets of Fig. 1). However, significant color changes to brown and black were observed for 570-ZIF-8 and 600-ZIF-8, indicating considerable decomposition and carbonization of ZIF-8 upon exposure to high temperatures.[59–61]

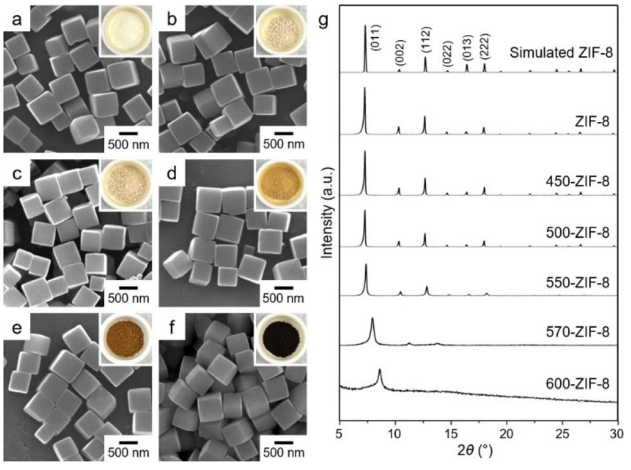

Fig. 1 SEM images of (a) ZIF-8, (b) 450-ZIF-8, (c) 500-ZIF-8, (d) 550-ZIF-8, (e) 570-ZIF-8, and (f) 600-ZIF-8. Photographs showing the color changes of T-ZIF-8 samples displayed in insets. (g) PXRD patterns of ZIF-8 and a series of T-ZIF-8 samples obtained after thermal treatment of ZIF-8 at varied temperatures.

3.2. Porous properties and surface charges of T-ZIF-8 samples

The change in the porosity of the T-ZIF-8 samples was examined by measuring the N_2 sorption isotherms at 77 K (Fig. 3a). In general, when MOFs undergo thermal treatment, their pore volumes and surface areas tend to decrease owing to the decomposition of MOFs.[49–51] This phenomenon was also observed in the T-ZIF-8 samples, as their N_2 sorption abilities gradually decreased with increasing temperature during the thermal treatment (Fig. 3a and Table S1†). Specifically, dramatic decreases in N_2 sorption were observed for 570-ZIF-8 and 600-ZIF-8. The Brunauer–Emmett–Teller (BET) surface areas of 570-ZIF-8 and 600-ZIF-8 were found to be 913.5 and 670.4 $m^2\ g^{-1}$ respectively, and their total pore volumes were 0.44 and 0.37 $cm^3\ g^{-1}$ respectively. These values are substantially lower than those of pure ZIF-8 at 1320.1 $m^2\ g^{-1}$ (BET surface area) and 0.67 $cm^3\ g^{-1}$ (total pore volume). However, no significant decrease in N_2 sorption was observed for 450-, 500-, and 550-ZIF-8. In addition, the pore size distributions (Fig. 3b) of 450- and 500-ZIF-8 calculated using the non-local density functional theory (NLDFT) method remained unchanged compared to the original ZIF-8, which exhibited the characteristic pore dimensions of ZIF-8 at approximately 11.6 Å.[22,62] Pore size of 10.4 Å was observed for 550-ZIF-8, which is slightly smaller than that of ZIF-8. However, the pore sizes of 570- and 600-ZIF-8 are significantly smaller than that of pure ZIF-8. In terms of pore volume, the thermal treatment of ZIF-8 is disadvantageous for the effective adsorption of the target molecule, as it results in a decrease in the adsorption capacity of the material.[49,50,59]

The surface charge of the adsorbent plays a crucial role in determining the effectiveness of the CWA simulant adsorption. In particular, the positive charge of MOFs enhances the adsorption of CWA simulants *via* effective polar interactions with the electron-rich atoms present in the molecules.[25,34,63,64]

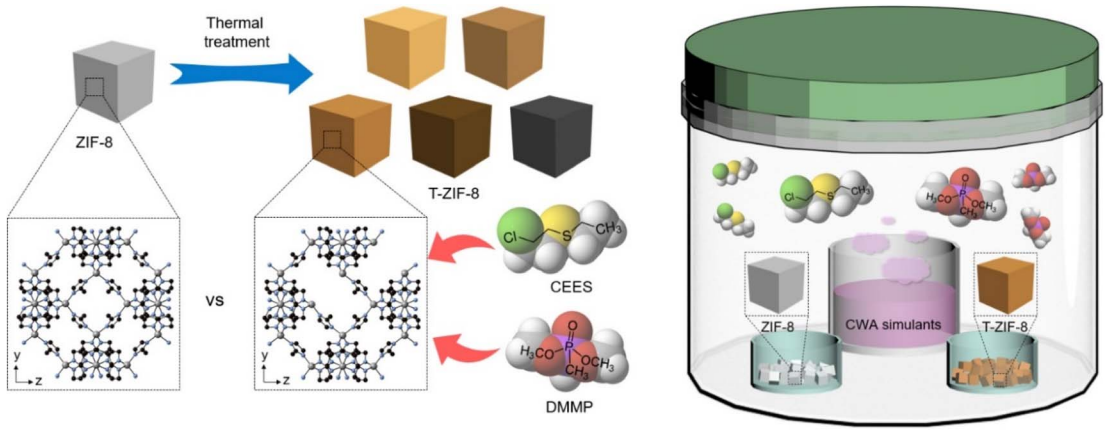

Fig. 2 Schematic illustration for the preparation of a series of T-ZIF-8 samples *via* the thermal treatment of ZIF-8 at varied temperatures (450, 500, 550, 570, and 600 °C). Schematic representation of a jar-in-jar setup for the adsorption experiment of CWA simulants (2-chloroethyl ethyl sulfide, CEES; or dimethyl methyl phosphonate, DMMP) on the ZIF-8 and T-ZIF-8 samples.

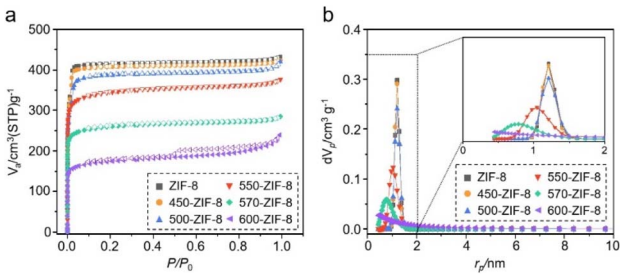

Fig. 3 (a) N_2 sorption isotherms of ZIF-8 and T-ZIF-8 samples; the filled and open symbols represent the adsorption and desorption branches, respectively. (b) Pore size distributions of ZIF-8 and T-ZIF-8 samples calculated using the NLDFT method.

We examined the change in the surface charges of T-ZIF-8 samples caused by the thermal treatment. Zeta-potential measurements indicated a gradual shift towards more positive surface charges for the T-ZIF-8 samples with increasing temperature (Fig. 4a). This can be understood by considering that thermal treatment of the MOF causes the decomposition of some of organic part, leading to the creation of open metal sites carrying a positive charge.[49–55] For example, pure ZIF-8 exhibited a surface charge at 28.7 mV; however, 550-ZIF, and 600-ZIF exhibited higher charges at 33.5 and 41.5 mV, respectively. Due to its large positive surface charge, T-ZIF-8 displayed the efficient adsorption of the negatively charged methyl orange (Fig. S2†). The binding energy of Zn 2p in the XPS spectra of the T-ZIF-8 samples shifted to a slightly higher position (Fig. 4c), while the binding energy of N 1s shifted to a slightly lower position (Fig. 4d) as the temperature increased, indicating an increase in Zn–N fractures.[49–51] The water contact angles of the T-ZIF-8 samples were measured to determine their hydrophilicity (Fig. 4b). In general, the contact angles decreased with an increase in temperature. The water contact angles of the ZIF-8 and five T-ZIF-8 samples were found to be 66, 61, 55, 48, 32, and 15°, respectively, indicating increased hydrophilicity of the surface of the T-ZIF-8 samples.

3.3. Adsorption of CWA simulants on T-ZIF-8 samples

The adsorption of CEES onto pure ZIF-8 and T-ZIF-8 was investigated using a jar-in-jar setup at room temperature (Fig. 1).[26] In this setup, small jars enclosing the ZIF-8 and T-ZIF-8 samples were placed in a large jar with CEES, and the ZIF samples were exposed to CEES vapors for various time intervals. After the exposure to CEES vapors, the ZIF samples were digested in a mixed deuterated solvent of dimethyl sulfoxide-d_6 and acetic acid-d_4, and the resulting solution was analyzed using ^{1}H NMR spectroscopy. Peak integrations of CEES and a standard molecule (CH_2Br_2) were used to determine the amount of CEES per gram of ZIF (Fig. S3 and S4†). The CEES

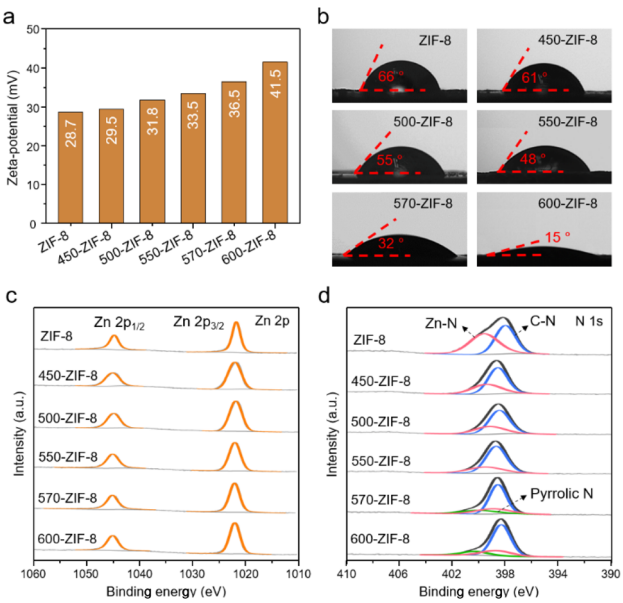

Fig. 4 (a) Zeta-potentials of ZIF-8 and T-ZIF-8 samples. (b) Water contact angle measurements of ZIF-8 and T-ZIF-8 samples. High-resolution (c) Zn 2p and (d) N 1s XPS profiles of ZIF-8 and T-ZIF-8 samples.

uptake was plotted against the exposure time of the ZIF samples (Fig. 5a). The amount of CEES adsorbed onto pure ZIF-8 was 417 mg of CEES per gram of ZIF-8 (417 $mg_{CEES}\ g_{adsorbent}^{-1}$). On the other hand, the adsorption abilities of porous carbon and zeolite have been reported to be 74 and 109 $mg_{CEES}\ g_{adsorbent}^{-1}$, respectively.[32,33] Thus, ZIF-8 outperforms other porous adsorbents by a considerable margin. It is worth noting that, with the exception of 600-ZIF-8, all the T-ZIF-8 samples exhibited improved CEES adsorption capacities compared to pure ZIF-8. Out of a series of T-ZIF-8 samples, 550-ZIF-8 displayed a 29% increase at 538 $mg_{CEES}\ g_{adsorbent}^{-1}$ in adsorption capacity compared with that of pure ZIF-8. However, excessive thermal treatment of ZIF-8 at high temperatures can lead to a decrease in its adsorption capacity by significantly reducing its porosity and surface area.[49,50,61] Indeed, 570- and 600-ZIF-8 displayed lower adsorption abilities than 550-ZIF-8 (Fig. 5). A particularly exciting outcome of this experiment was the significant improvement in CEES adsorption observed in T-ZIF-8 during the early stage of exposure to CEES vapors. Except 600-ZIF-8, all the T-ZIF-8 samples demonstrated dramatically enhanced CEES adsorption capacities during the first 15 min of exposure to CEES vapors (Fig. 5b). Notably, 550-ZIF-8 exhibited an impressive 216% increase in the early-stage adsorption compared to that of pure ZIF-8 (Fig. 5b and c). This improvement can be attributed to the positive surface charge and the availability of open metal sites in the T-ZIF-8s. Specifically, the enhanced ability to adsorb CEES can be attributed to T-ZIF-8's effective polar interactions with the electron-rich sulfur atoms in CEES.[25,34,63,64] The positive charge of the adsorbent enhances this interaction with the electron-rich sulfur atoms in CEES, thereby enhancing the adsorption capacity. These results highlighted the potential of T-ZIF-8 as a highly effective material for the rapid adsorption of CWAs. The ability to adsorb CWAs during the early stage of exposure, more than the maximum adsorption capacity during saturation, is crucial for the fast removal or detection of CWAs, given the critical nature of this concern.

The successful adsorption of CEES onto the ZIF samples was confirmed using IR and EDX spectroscopy. Specifically, the IR spectra of the ZIF samples after exposure to and adsorption of CEES vapors displayed characteristic IR bands for CEES at 1262.2 and 1213.0 cm^{-1} (Fig. S5†).[25,65] Additionally, the EDX spectra of the ZIF samples showed the presence of sulfur and chlorine originated from CEES (Fig. S6†). The SEM images and PXRD patterns of the ZIF-8 samples after CEES adsorption revealed no critical morphological or structural changes (Fig. S7 and S8†).

To further investigate the efficacy of T-ZIF-8 for CEES adsorption, the recyclability of the material was examined through three consecutive adsorption measurements (Fig. 6a). These results demonstrate that the CEES adsorption capacity of 550-ZIF-8 remained consistent during the three adsorption cycles. Furthermore, the SEM image and PXRD pattern (Fig. 6b and c, respectively) of 550-ZIF-8 after three adsorption cycles show no critical morphological or structural changes, which suggests that 550-ZIF-8 is a highly effective and stable material for CEES adsorption.

In addition, the DMMP adsorption abilities of the pure ZIF-8 and T-ZIF-8 samples were analyzed by measuring the DMMP uptake using the same jar-in-jar setup. The ZIF samples exposed to DMMP vapors for different time spans were digested in a mixed deuterated solvent, and the peak integrations of DMMP and the internal standard (CH_2Br_2) were used to determine the amounts of DMMP in the ZIF samples (Fig. S9 and S10†). The adsorption of DMMP on the ZIF samples was confirmed through the IR and EDX spectra (Fig. S11 and S12†). The IR spectra of the ZIF samples after exposure to and adsorption of DMMP vapors displayed the characteristic IR bands of DMMP (Fig. S11†). Additionally, the EDX spectra of the ZIF samples showed the presence of phosphorus from DMMP (Fig. S12†). Adsorption graphs showing the DMMP uptake are presented in

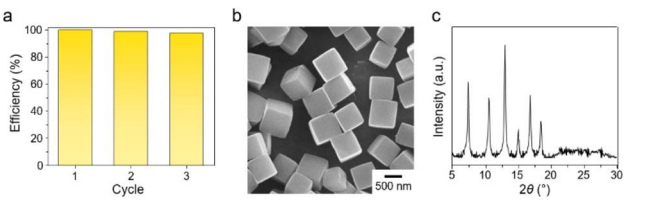

Fig. 6 (a) Recyclability of 550-ZIF-8 over three successive CEES adsorption cycles. Second and third cycles were run after removal of the adsorbed CEES *via* the immersion of the sample in methanol. (b) SEM image and (c) PXRD pattern of 550-ZIF-8 after three successive adsorption cycles.

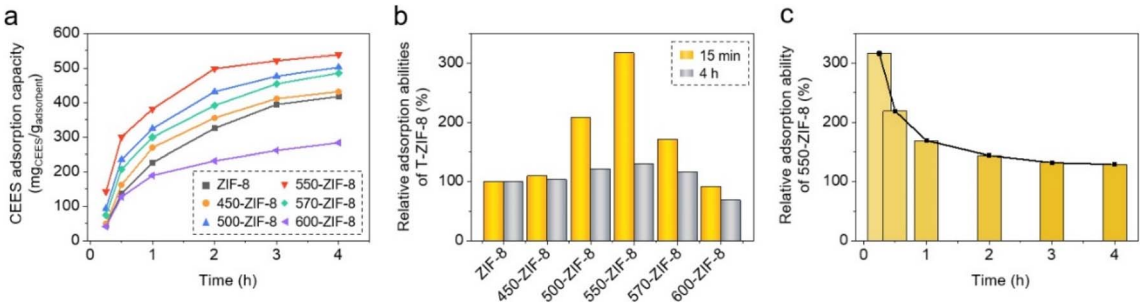

Fig. 5 (a) Time-dependent CEES adsorption plots for pure ZIF-8 and T-ZIF-8 samples. (b) Relative adsorption abilities of T-ZIF-8 samples compared to pure ZIF-8 at the early stage (15 min) and saturated stage (4 h) of exposure to CEES vapors. (c) Relative adsorption ability of 550-ZIF-8 compared to pure ZIF-8 after the exposure to CEES vapors at different time durations.

Fig. 7a. The saturation of DMMP adsorption in ZIF-samples took 5 day, which was significantly longer than the time taken for the saturation of CEES adsorption, that is, 4 h. This is due to the lower vapor pressure of DMMP, 0.96 mmHg at 25 °C, compared to a vapor pressure of 3.4 mmHg for CEES, at the same temperature.[66,67] The amount of DMMP adsorbed on pure ZIF-8 was found to be 416 mg per gram of ZIF-8 (416 mg_{DMMP} $g_{adsorbent}^{-1}$). This capacity is comparable to those of other porous adsorbents. For example, the adsorption ability of other MOF (Zr-abtc) and porous carbon has been reported to be 351 and 460 mg_{DMMP} $g_{adsorbent}^{-1}$, respectively.[20,29] In addition, all the T-ZIF-8 samples exhibited improved DMMP adsorption capacities similar to that of CEES, compared to pure ZIF-8, except for 600-ZIF-8. Among them, 550-ZIF-8 displayed the highest increase (31%) in adsorption compared to that for pure ZIF-8. Importantly, a dramatic improvement in DMMP adsorption was found for T-ZIF-8 during the early stage of exposure to DMMP vapors. All the T-ZIF-8 samples exhibited superior DMMP adsorption capacities during the first 1 h of exposure to DMMP vapors, with the exception of 600-ZIF-8 (Fig. 7b). Especially, 550-ZIF-8 demonstrated an outstanding 185% increase in adsorption compared to pure ZIF-8 (Fig. 7b and c). SEM images and PXRD patterns showed no morphological or structural changes after DMMP adsorption, indicating that the ZIF samples retained their original properties (Fig. S13†). Furthermore, the adsorption kinetics of pure ZIF-8 and T-ZIF-8 samples were shown in Fig. S14 and Table S2.† The adsorption of CEES and DMMP on ZIF-8 and T-ZIF-8 samples was fitted to the pseudo-first order model, and kinetics of CEES adsorption was faster than DMMP adsorption. This indicated that DMMP adsorption process required a longer time to reach the equilibrium adsorption amount. The adsorption ability of 550-ZIF-8 in the presence of both CEES and DMMP was investigated *via* placing a 550-ZIF-8 sample in a large jar with both CEES and DMMP. After 1 h exposure to both CEES and DMMP vapors, 550-ZIF-8 sample holds 345 mg_{CEES} $g_{adsorbent}^{-1}$ and 25 mg_{DMMP} $g_{adsorbent}^{-1}$, respectively.

3.4. Catalytic degradation of DMMP using 550-ZIF-8

The catalytic degradation of DMMP using pure ZIF-8 and 550-ZIF-8 was investigated. It was anticipated that 550-ZIF-8 would exhibit an improved catalytic performance compared to ZIF-8 due to its enhanced adsorption capability during the early stages of exposure to DMMP. DMMP can be hydrolyzed by the catalyst to form methylphosphonic acid (MPA).[21,40–42] The progression of the reaction was analyzed using ^{31}P NMR spectroscopy. Peak integrations of DMMP and MPA were utilized to determine the conversion rate (Fig. 8, S15, and S16†). Initially, a background reaction without any catalyst was conducted, which resulted in only 2% conversion over 72 h. On the other hand, ZIF-8 exhibited a conversion rate of 26% over the same 72 h reaction time. However, the catalytic activity of 550-ZIF-8 for the hydrolysis of DMMP was significantly enhanced, achieving a conversion rate of 67% over 72 h (Fig. 8). This improvement was attributed to the significantly enhanced adsorption capacity of 550-ZIF-8, leading to higher conversion rates. The reaction mechanism for degradation of DMMP was well established in two steps; (i) the initial interaction of phosphate group of DMMP with the Lewis acid site of catalyst, (ii) subsequent nucleophilic attack by water.[22,68,69] However, no critical catalytic degradation of DMMP in the presence of 550-ZIF-8 was observed at room temperature. In addition, the catalytic degradation of dimethyl 4-nitrophenylphosphate using 550-ZIF-8 was conducted in aqueous

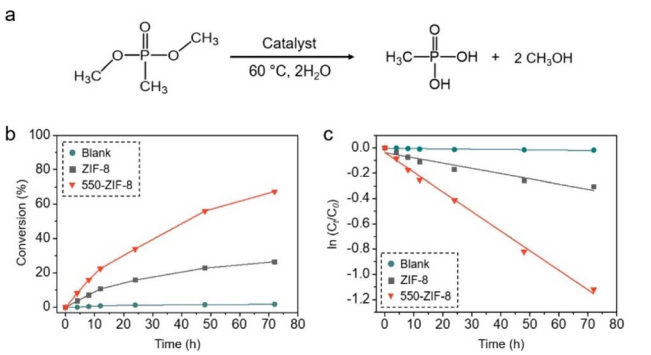

Fig. 8 (a) Hydrolytic decomposition of DMMP to MPA. (b) The plots for the conversions of DMMP to MPA with or without catalysts (ZIF-8 and 550-ZIF-8) in varied time points. (c) Linear relationships between $\ln(C_t/C_0)$ and reaction time in the absence of catalysts and in the presence of ZIF-8 and 550-ZIF-8. C_0 and C_t represent the amounts of DMMP at the initial stage and time t, respectively.

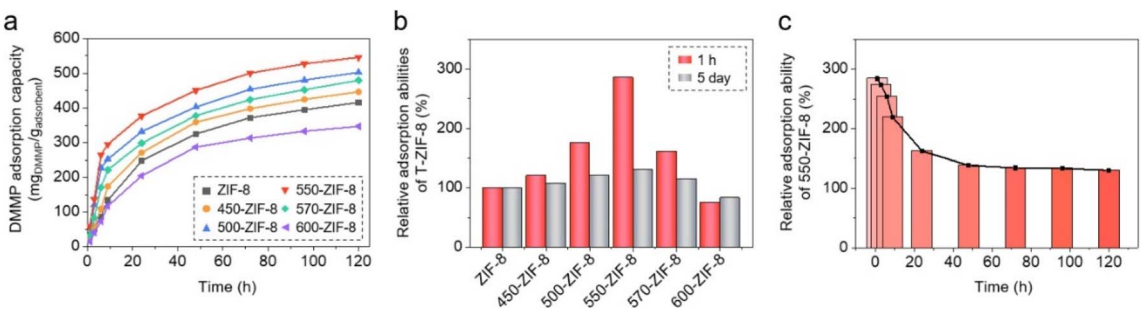

Fig. 7 (a) Time-dependent DMMP adsorption plots for pure ZIF-8 and T-ZIF-8 samples. (b) Relative adsorption abilities of a series of T-ZIF-8 compared to pure ZIF-8 at the early stage (1 h) and saturated stage (5 day) of exposure to DMMP vapors. (c) Relative adsorption ability of 550-ZIF-8 compared to pure ZIF-8 after the exposure to DMMP vapors at different time durations.

buffer solution at room temperature.[26,70,71] 550-ZIF-8 exhibited a conversion rate 84% over the 72 h reaction time (Fig. S17 and S18†).

4. Conclusions

The efficient removal of hazardous substances, such as CWAs, from the environment is of paramount importance for mitigating the significant risks they pose to both humans and ecosystems. Adsorption has emerged as an effective method for addressing this challenge, and the development of porous materials with strong CWA adsorption capabilities is a crucial step toward safeguarding human lives. In this regard, the use of thermally treated ZIF-8 (T-ZIF-8) is a remarkable advancement in the efficient adsorption of CWA simulants. By subjecting ZIF-8 to a simple thermal treatment, T-ZIF-8 samples were prepared, resulting in several notable changes. The surface charge of T-ZIF-8 became more positive with open metal sites. These modifications positively influenced the adsorption capacity of CWA simulants by T-ZIF-8. Although the pore volume of T-ZIF-8 decreased after the thermal treatment, the positive surface charge were advantageous for adsorption. The most important finding was that T-ZIF-8 exhibited a significantly enhanced adsorption ability during the early stage of exposure to CWA simulants. This improvement can be attributed to the effective polar interactions between T-ZIF-8 and the simulants facilitated by the electron-rich components within the CWA simulants. T-ZIF-8 demonstrated excellent stability over three adsorption cycles, confirming its suitability for long-term applications. Furthermore, enhanced adsorption ability of T-ZIF-8 led to its improved activity for the degradation of simulant. Overall, the advances in the adsorption of CWA simulants using T-ZIF-8 present a promising prospect for the efficient removal of hazardous substances. T-ZIF-8 exhibits high adsorption effectiveness, particularly in the early stage of exposure, and maintains excellent stability over repeated adsorption cycles. These findings suggest that T-ZIF-8 is an outstanding material for early-stage removal of CWA simulants, offering both high efficacy and stability in the remediation of hazardous environments.

Author contributions

Moonhyun Oh designed, coordinated the research, and drafted the manuscript. Sojin Oh, Sujeong Lee, and Gihyun Lee conducted experiments. Sojin Oh, Sujeong Lee, Gihyun Lee, and Moonhyun Oh conducted data analysis and revised the manuscript. The authors read and approved the final manuscript.

Conflicts of interest

There are no conflicts to declare.

Acknowledgements

This research was supported by the Challengeable Future Defense Technology Research and Development Program through the Agency for Defense Development (ADD) funded by the Defense Acquisition Program Administration (DAPA) in 2023 (No. 915019201) and by the National Research Foundation of Korea (NRF) grant funded by the Korea government (MSIT) (no. NRF-2022R1A2B5B03001450).

References

1 G. Cai, P. Yan, L. Zhang, H. C. Zhou and H. L. Jiang, *Chem. Rev.*, 2021, **121**, 12278–12326.
2 M. Ding, R. W. Flaig, H. L. Jiang and O. M. Yaghi, *Chem. Soc. Rev.*, 2019, **48**, 2783–2828.
3 K. Nath, A. Ahmed, D. J. Siegel and A. J. Matzger, *J. Am. Chem. Soc.*, 2022, **144**, 20939–20946.
4 J. Liu, T. A. Goetjen, Q. Wang, J. G. Knapp, M. C. Wasson, Y. Yang, Z. H. Syed, M. Delferro, J. M. Notestein, O. K. Farha and J. T. Hupp, *Chem. Soc. Rev.*, 2022, **51**, 1045–1097.
5 H. Yoon, S. Lee, S. Oh, H. Park, S. Choi and M. Oh, *Small*, 2019, **15**, 1805232.
6 H. Jun, S. Oh, G. Lee and M. Oh, *Sci. Rep.*, 2022, **12**, 14735.
7 J. J. Pang, Z. Q. Yao, K. Zhang, Q. W. Li, Z. X. Fu, R. Zheng, W. Li, J. Xu and X. H. Bu, *Angew. Chem., Int. Ed.*, 2023, **62**, e202217456.
8 T. Y. Luo, P. Das, D. L. White, C. Liu, A. Star and N. L. Rosi, *J. Am. Chem. Soc.*, 2020, **142**, 2897–2904.
9 W. Cho, H. J. Lee, G. Choi, S. Choi and M. Oh, *J. Am. Chem. Soc.*, 2014, **136**, 12201–12204.
10 C. S. Smoljan, Z. Li, H. Xie, C. J. Setter, K. B. Idrees, F. A. Son, F. Formalik, S. Shafaie, T. Islamoglu, L. K. Macreadie, R. Q. Snurr and O. K. Farha, *J. Am. Chem. Soc.*, 2023, **145**, 6434–6441.
11 M. I. Gonzalez, M. T. Kapelewski, E. D. Bloch, P. J. Milner, D. A. Reed, M. R. Hudson, J. A. Mason, G. Barin, C. M. Brown and J. R. Long, *J. Am. Chem. Soc.*, 2018, **140**, 3412–3422.
12 S. Zhou, O. Shekhah, A. Ramírez, P. Lyu, E. Abou-Hamad, J. Jia, J. Li, P. M. Bhatt, Z. Huang, H. Jiang, T. Jin, G. Maurin, J. Gascon and M. Eddaoudi, *Nature*, 2022, **606**, 706–712.
13 Y. Gu, J. J. Zheng, K. i. Otake, M. Shivanna, S. Sakaki, H. Yoshino, M. Ohba, S. Kawaguchi, Y. Wang, F. Li and S. Kitagawa, *Angew. Chem., Int. Ed.*, 2021, **60**, 11688–11694.
14 H. S. Cho, H. Deng, K. Miyasaka, Z. Dong, M. Cho, A. V. Neimark, J. K. Kang, O. M. Yaghi and O. Terasaki, *Nature*, 2015, **527**, 503–507.
15 M. Woellner, S. Hausdorf, N. Klein, P. Mueller, M. W. Smith and S. Kaskel, *Adv. Mater.*, 2018, **30**, 1704679.
16 T. Islamoglu, Z. Chen, M. C. Wasson, C. T. Buru, K. O. Kirlikovali, U. Afrin, M. R. Mian and O. K. Farha, *Chem. Rev.*, 2020, **120**, 8130–8160.
17 N. S Bobbitt, M. L. Mendonca, A. J. Howarth, T. Islamoglu, J. T. Hupp, O. K. Farha and R. Q. Snurr, *Chem. Soc. Rev.*, 2017, **46**, 3357–3385.
18 N. Couzon, J. Dhainaut, C. Campagne, S. Royer, T. Loiseau and C. Volkringer, *Coord. Chem. Rev.*, 2022, **467**, 214598.

19 C. Montoro, F. Linares, E. Q. Procopio, I. Senkovska, S. Kaskel, S. Galli, N. Masciocchi, E. Barea and J. A. R Navarro, *J. Am. Chem. Soc.*, 2011, **133**, 11888–11891.
20 S. K. Chitale, Y. S. Ko, J. W. Choi, J. W. Yoon, D. Jo, S. K. Lee, K. H. Cho and U. H. Lee, *J. Hazard. Mater. Lett.*, 2022, **3**, 100066.
21 F. J. Ma, S. X. Liu, C. Y. Sun, D. D. Liang, G. J. Ren, F. Wei, Y. G. Chen and Z. M. Su, *J. Am. Chem. Soc.*, 2011, **133**, 4178–4181.
22 A. M. Ebrahim, A. M. Plonka, N. Rui, S. Hwang, W. O. Gordon, A. Balboa, S. D. Senanayake and A. I. Frenkel, *ACS Appl. Mater. Interfaces*, 2020, **12**, 58326–58338.
23 K. Ma, T. Islamoglu, Z. Chen, P. Li, M. C. Wasson, Y. Chen, Y. Wang, G. W. Peterson, J. H. Xin and O. K. Farha, *J. Am. Chem. Soc.*, 2019, **141**, 15626–15633.
24 F. A. Son, M. C. Wasson, T. Islamoglu, Z. Chen, X. Gong, S. L. Hanna, J. Lyu, X. Wang, K. B. Idrees, J. J. Mahle, G. W. Peterson and O. K. Farha, *Chem. Mater.*, 2020, **32**, 4609–4617.
25 P. Asha, M. Sinha and S. Mandal, *RSC Adv.*, 2017, **7**, 6691–6696.
26 T. Wu, F. Qiu, R. Xu, Q. Zhao, L. Guo, D. Chen, C. Li and X. Jiao, *ACS Appl. Mater. Interfaces*, 2023, **15**, 1265–1275.
27 Y. R. Son, S. G. Ryu and H. S. Kim, *Microporous Mesoporous Mater.*, 2020, **293**, 109819.
28 C. Zhou, B. Yuan, S. Zhang, G. Yang, L. Lu, H. Li and C. A. Tao, *ACS Appl. Mater. Interfaces*, 2022, **14**, 23383–23391.
29 K. Huynh, S. Holdren, J. Hu, L. Wang, M. R. Zachariah and B. W. Eichhorn, *ACS Appl. Mater. Interfaces*, 2017, **9**, 40638–40644.
30 D. A. Giannakoudakis, M. Barczak, M. Florent and T. J. Bandosz, *Chem. Eng. J.*, 2019, **362**, 758–766.
31 E. J. Park, H. J. Kim, S. W. Han, J. H. Jeong, I. H. Kim, H. O. Seo and Y. D. Kim, *Chem. Eng. J.*, 2017, **325**, 433–441.
32 M. Florent, D. A. Giannakoudakis, R. Wallace and T. J. Bandosz, *ACS Appl. Mater. Interfaces*, 2017, **9**, 26965–26973.
33 Y. R. Son, M. K. Kim, S. G. Ryu and H. S. Kim, *ACS Appl. Mater. Interfaces*, 2018, **10**, 40651–40660.
34 M. Sadeghi, S. Yekta and D. Mirzaei, *J. Alloys Compd.*, 2018, **748**, 995–1005.
35 W. A. Khanday, *Microporous Mesoporous Mater.*, 2017, **244**, 15–20.
36 H. Jung, M. K. Kim, J. Lee, J. H. Kwon and J. Lee, *Anal. Lett.*, 2021, **54**, 468–480.
37 T. Islamoglu, A. Atilgan, S. Y. Moon, G. W. Peterson, J. B. DeCoste, M. Hall, J. T. Hupp and O. K. Farha, *Chem. Mater.*, 2017, **29**, 2672–2675.
38 Y. Li, Q. Gao, Y. Zhou, L. Zhang, Y. Zhong, Y. Ying, M. Zhang, Y. Liu and Y. Wang, *J. Hazard. Mater.*, 2018, **358**, 113–121.
39 M. K. Kim, S. H. Kim, M. Park, S. G. Ryu and H. Jung, *RSC Adv.*, 2018, **8**, 41633–41638.
40 W. Guo, H. Lv, K. P. Sullivan, W. O. Gordon, A. Balboa, G. W. Wagner, D. G. Musaev, J. Bacsa and C. L. Hill, *Angew. Chem., Int. Ed.*, 2016, **55**, 7403–7407.
41 Y. L. Wu, Y. Q. Sun, X. X. Li and S. T. Zheng, *Inorg. Chem. Commun.*, 2020, **113**, 107815.
42 M. Sadeghi, H. Ghaedi, S. Yekta and E. Babanezhad, *J. Environ. Chem. Eng.*, 2016, **4**, 2990–3000.
43 Y. Sun, A. Spieß, C. Jansen, A. Nuhnen, S. Gökpinar, R. Wiedey, S.-J. Ernst and C. Janiak, *J. Mater. Chem. A*, 2020, **8**, 13364–13375.
44 H. Zhao, Q. Wang, Z. Xi, C. Liu and C. Miao, *J. Solid State Chem.*, 2023, **324**, 124135.
45 H. S. AlSalem, F. K. Algethami, S. T. Al-Goul and A. Shahat, *ACS Omega*, 2023, **8**, 20125–20137.
46 A. A. G. Khamseh, S. A. Ghorbanian, Y. Amini and M. M. Shadman, *Sci. Rep.*, 2023, **13**, 8393.
47 M. L. Gao, L. Li, Z. X. Sun, J. R. Li and H. L. Jiang, *Angew. Chem., Int. Ed.*, 2022, **61**, e202211216.
48 X. Y. Liu, W. S. Lo, C. Wu, B. P. Williams, L. Luo, Y. Li, L. Y. Chou, Y. Lee and C. K. Tsung, *Nano Lett.*, 2020, **20**, 1774–1780.
49 J. D. Xiao, Q. N. Wang, Z. D. Feng, S. Tang, Y. Liu and C. Li, *J. Catal.*, 2022, **406**, 165–173.
50 S. Gadipelli, W. Travis, W. Zhou and Z. Guo, *Energy Environ. Sci.*, 2014, **7**, 2232–2238.
51 Y. Yun, Y. Fang, W. Fu, W. Du, Y. Zhu, H. Sheng, D. Astruc and M. Zhu, *Small*, 2022, **18**, 2107459.
52 J. Zhang, M. Zou, Q. Li, W. Dai, D. Wang, S. Zhang, B. Li, L. Yang, S. Luo and X. Luo, *Appl. Surf. Sci.*, 2022, **572**, 151408.
53 S. Chen, S. Mukherjee, B. E. G. Lucier, Y. Guo, Y. T. A. Wong, V. V. Terskikh, M. J. Zaworotko and Y. Huang, *J. Am. Chem. Soc.*, 2019, **141**, 14257–14271.
54 L. Xiang, H. Zhang, C. Huang, R. Fei, X. Hu and J. Li, *Colloids Surf., A*, 2023, **662**, 131042.
55 P. Wu, Y. Shen, H. Li, W. Shi, L. Zhang, T. Pan, W. Pei, W. Zhang and F. Huo, *Small Struct.*, 2021, **2**, 2000119.
56 C. Wang, Y. Yao, J. Li and Y. Yamauchi, *Acc. Mater. Res.*, 2022, **3**, 426–438.
57 P. He, W. Ma, J. Xu, J. Wei, X. Liu, P. Zuo, Z. K. Cui and Q. Zhuang, *Small*, 2023, **19**, 2204649.
58 H. Park, S. Oh, S. Lee, S. Choi and M. Oh, *Appl. Catal., B*, 2019, **246**, 322–329.
59 S. Oh, S. Lee and M. Oh, *ACS Appl. Mater. Interfaces*, 2020, **12**, 18625–18633.
60 S. Choi and M. Oh, *Angew. Chem., Int. Ed.*, 2019, **58**, 866–871.
61 S. Tanaka and Y. Tanaka, *ACS Omega*, 2019, **4**, 19905–19912.
62 K. S. Park, Z. Ni, A. P. Côté, J. Y. Choi, R. Huang, F. J. Uribe-Romo, H. K. Chae, M. O'Keeffe and O. M. Yaghi, *Proc. Natl. Acad. Sci. U. S. A.*, 2006, **103**, 10186–10191.
63 J. A. Arcibar-Orozco, S. Panettieri and T. J. Bandosz, *J. Mater. Chem. A*, 2015, **3**, 17080–17090.
64 D. B. Mawhinney, J. A. Rossin, K. Gerhart and J. T. Yates Jr, *Langmuir*, 1999, **15**, 4789–4795.
65 T. L. Thompson, D. A. Panayotov and J. T. Yates Jr, *J. Phys. Chem. B*, 2004, **108**, 16825–16833.
66 A. B. Butrow, J. H. Buchanan and D. E. Tevault, *J. Chem. Eng. Data*, 2009, **54**, 1876–1883.
67 M. Spiandore, A. Piram, A. Lacoste, D. Josse and P. Doumenq, *Drug Test. Anal.*, 2014, **6**, 67–73.

68 G. Wang, G. Sharp, A. M. Plonka, Q. Wang, A. I. Frenkel, W. Guo, C. Hill, C. Smith, J. Kollar, D. Troya and J. R. Morris, *J. Phys. Chem. C*, 2017, **121**, 11261–11272.
69 Q. Hu, V. M. Jayasinghe-Arachchige, J. Zuchniarz and R. Prabhakar, *Front. Chem.*, 2019, **7**, 195.
70 S. Y. Moon, Y. Liu, J. T. Hupp and O. K. Farha, *Angew. Chem., Int. Ed.*, 2015, **54**, 6795–6799.
71 Z. Chen, T. Islamoglu and O. K. Farha, *ACS Appl. Nano Mater.*, 2019, **2**, 1005–1008.